HHS Public Access

Author manuscript

Magn Reson Med. Author manuscript; available in PMC 2017 March 01.

Published in final edited form as:

Magn Reson Med. 2016 March ; 75(3): 1341–1345. doi:10.1002/mrm.25709.

The Microstructural Correlates of T_1 in White Matter

Kevin D. Harkins[1], **Junzong Xu**[1,2], **Adrienne N. Dula**[1,2], **Ke Li**[1], **William M Valentine**[3], **Daniel F. Gochberg**[1,2,4], **John C. Gore**[1,2,4,5,6], and **Mark D. Does**[1,2,5,7]

[1]Institute of Imaging Science, Vanderbilt University

[2]Department of Radiology and Radiological Sciences, Vanderbilt University

[3]Department of Pathology, Vanderbilt University

[4]Department of Physics and Astronomy, Vanderbilt University

[5]Department of Biomedical Engineering, Vanderbilt University

[6]Department of Molecular Physiology and Biophysics, Vanderbilt University

[7]Department of Electrical Engineering, Vanderbilt University

Abstract

Purpose—Several studies have shown strong correlations between myelin content and T_1 within the brain, and have even suggested that T_1 can be used to estimate myelin content. However, other micro-anatomical features such as compartment size are known to affect longitudinal relaxation rates, similar to compartment size effects in porous media.

Methods—T_1 measurements were compared with measured or otherwise published axon size measurements in white matter tracts of the rat spinal cord, rat brain, and human brain.

Results—In both ex vivo and in vivo studies, correlations were present between the relaxation rate $1/T_1$ and axon size across regions of rat spinal cord with nearly equal myelin content.

Conclusions—While myelination is likely the dominant determinant of T_1 in white matter, variations in white matter microstructure, independent of myelin volume fraction, may also be reflected in T_1 differences between regions or subjects.

Keywords

rat; spinal cord; T_1; axon size; MRI; microstructure

INTRODUCTION

In magnetic resonance imaging (MRI), the longitudinal relaxation rate ($R_1=1/T_1$) is the primary source of contrast in many protocols, particularly for neurological MRI. T_1 differences between gray matter and white matter are well established (1,2) and often attributed to the presence of myelin (3), a dielectric material containing lipid membranes,

All correspondence should be addressed to: Mark D. Does, Ph.D., 1161 21st Ave South, AA-1105, Nashville, TN 37232-2310, Ph: 615-322-8352, mark.does@vanderbilt.edu.

cholesterol, proteins, and water that coats axons to increase conduction velocity of an action potential. Water that is present in myelin is thought to exhibit a lower T_1 than non-myelin water (3-7); thus, an increase in the volume fraction of myelin will reduce the average T_1 of white matter. Consistent with known changes in myelination, T_1 decreases in developing brain, especially in white matter (8,9), and decreases in neurological disease involving loss of myelin, including multiple sclerosis (10). Similarly, regional variations in myelin content have been correlated with variations in T_1 (11-13), and recent studies demonstrate the potential for T_1 measurements to serve as a quantitative marker for myelin content (14,15).

Still, the underlying characteristics of tissue that determine T_1 in the brain, including the role of myelin, are not fully understood, and may include both molecular and microstructural factors. For instance, it has been shown that structure size can affect T_1 and T_2 in porous media through surface relaxation effects (16), and the rate of water exchange between myelin and non-myelin components of white matter is thought to influence T_2 (17,18). It is possible that T_1 is similarly affected by compartment size and/or inter-compartmental water exchange. This work explores the relationship between T_1 and microstructural characteristics of white matter, specifically axon size, through comparisons of T_1 measurements in the rat spinal cord and corpus callosum with quantitative histology.

METHODS

All animal studies involved Sprague Dawley rats and were approved by the Vanderbilt University Institutional Animal Care and Use Committee. Measurements of T_1 from spinal cord (ex vivo and in vivo) and corpus callosum (in vivo) were made and compared with quantitative histological measures of white matter microstructure.

Spinal Cord MRI

The spinal cord data were acquired as part of previously published studies (17,18) and retrospectively analyzed in this paper. Water proton T_1 was measured in each spinal cord using a selective inversion-recovery prepared fast spin echo pulse sequence (19), with a hard inversion pulse (1-1.5 ms), echo train length of 16, 5.6 ms echo spacing, and 25 inversion-recovery times (t_{IR}) pseudo-logarithmically spaced between 3.5 ms and 10 s. The pre-delay (T_D) was 3.5 s, and 2 averages were collected for each scan.

Ex vivo—MR imaging was performed on 6 male rats with a 7 Tesla (T), 16 cm bore Agilent/Varian DirectDrive Console (Santa Clara, CA), and a 10 mm loop gap coil was used for excitation and reception. A 2 mm slice was scouted transverse to the spinal cord at the C2 level, and T_1 measurements were made over a 5×5 mm^2 field-of-view (FOV), encoded with 64×64 samples, then reconstructed to 128×128 by zero-padding.

In vivo—MR imaging was performed on 8 female rats with a 9.4 T Agilent/Varian DirectDrive Console (Santa Clara, CA), and a 38 mm Litz quadrature coil (Doty Scientific, Columbia, SC) was used for excitation and reception. Rats were imaged under isoflurane anesthesia with respiration rate monitored and body temperature maintained near 37 °C. From a scout image, a 1.5 mm slice was selected transverse to the cervical spinal cord, and

T_1 measurements were made over a 25.6 × 25.6 mm^2 FOV encoded with 128 × 128 samples.

Analysis—For both in vivo and ex vivo studies, regions of interest (ROIs) were drawn on the dorsal cortical spinal (dCST), funiculus gracilis (FG), rubrospinal (RST), and vestibulospinal cord (VST) tracts. For ex vivo studies, where resolution within the spinal cord was higher, additional ROIs were drawn on the funiculus cutaneous (FC) and reticulospinal cord (ReST) tracts. In vivo images from each t_{IR} were rigidly co-registered (20). Mean signal intensities from each ROI were fitted as a function of t_{IR} to a five-parameter quantitative magnetization transfer (qMT) model describing longitudinal magnetization and exchange within a two-pool system or water and macromolecular protons (19,21). T_1 and macromolecular pool-size ratio (PSR) were tabulated across ROIs. Correlations between $1/T_1$ and axon size or myelin fraction were calculated from ROI based means. Due to the uniform structure of the spinal cord through the prescribed slice, the signal from each ROI was assumed to originate from white matter only, without partial volume contributions from CSF.

Brain MRI

For in-vivo evaluation of the corpus callosum, a rat was imaged using the same 9.4 T magnet and coil described above. From scout images, a 1 mm sagittal slice was selected through the center of the rat brain. T_1 was measured with an inversion-recovery prepared spin echo sequence with echo time = 6 ms and 7 t_{IR} values pseudo-logarithmically spaced between 0.10 and 2.50 s, and T_D = 3.5 s. A 32 × 32 mm^2 FOV was encoded with 128 × 128 samples. Similar measurements were made in the human corpus callosum on a Philips (Best, NL) Achieva 3T scanner. Human studies were approved by the Vanderbilt Institutional Review Board. T_1 was measured using an inversion-recovery prepared turbo spin echo sequence with echo spacing = 6.8 ms, 12 echoes, 8 t_{IR} values log-spaced between 0.05 s and 6 s, and T_D = 3.5 s. A single 5 mm thick sagittal slice was encoded with 192 × 192 samples over 19.2 × 19.2 mm^2. For both rat and human data, signal magnitudes as a function of t_{IR} and T_D were used to estimate T_1 and inversion pulse flip angle.

Histology

Histology images were collected in the same spinal cord tracts evaluated by MRI, and 6 samples from the ex-vivo study & 3 samples from the in-vivo study were processed as previously published (17,18). The mean axon diameter was measured on 40-100 randomly selected axons by taking the arithmetic average of the inner long and short axis measurements. The myelin fraction was evaluated across animals and ROIs by semi-automatic segmentation of the histology images into regions of myelin and non-myelin compartments.

RESULTS

Within the ex vivo study, histologically derived mean axon size and myelin content are given in Table 1, as well as MRI measured qMT parameters, T_1 and PSR. All data and error bars are given +/− the inter-subject standard deviation, which dominated over intra-ROI

uncertainty. Summary scatter plots between histology parameters and R_1 (= $1/T_1$) are shown in Fig 1. Similarly, for the in vivo spinal cord study, histological and MRI derived parameters are also given in Table 1, with scatter plots given in Fig 2. Both ex vivo and in vivo studies demonstrate a correlation of R_1 with axon size, while no trend is evident with myelin content. A cropped mid-sagittal slice of the rat brain is shown in Fig 3 with an overlay showing the measured R_1 values across the corpus callosum. R_1 is lowest on the posterior portion of the midbody. Similarly, a mid-sagittal view of the human brain with overlay showing R_1 values across the corpus callosum is shown in Fig 4.

DISCUSSION

The present study illuminates a relationship between microstructural feature size in white matter and T_1. In both ex vivo and in vivo spinal cord studies, R_1 variations across tracts correlated with regional changes in axon size. No significant correlation was found between R_1 and myelin content possibly due to the small range in myelin content present within the spinal cord tracts analyzed, although another study showed a significant correlation between T_1 and both myelinated axons & axon size in a mouse model of demyelination (22). In the present work, Figs 1 and 2 demonstrate that R_1 correlates with average axon size and that axon size variations in the rat spinal cord are responsible for changes in $R_1 \approx 0.05\ s^{-1}$ in vivo and $\approx 0.15\ s^{-1}$ ex vivo. For comparison, Stüber et al. report changes in $R_1 \approx 0.33\ s^{-1}$ across a range of myelin volume fractions of 0 to 0.5 in human brain ex vivo (14). It should be noted that the R_1 measurements from both the in vivo and ex vivo spinal cord studies were derived from a qMT analysis of inversion-recovery measurements (a bi-exponential model). However, re-analysis of these data using only a sub-set of inversion times typical of a mono-exponential T_1 measurement (not shown) resulted in a similar relationship between R_1 and axon size.

The in vivo rat brain data, which was collected with a conventional inversion-recovery sequence and analyzed as a mono-exponential T_1, shows a trend that is consistent with those observed from spinal cord. Figure 3 shows that within the corpus callosum, R_1 is lower in the posterior portion of the midbody ($\approx$ 0.65 1/s) than the anterior midbody ($\approx$ 0.71 1/s). Although these values may also be affected by variations in myelin content, this trend in R_1 agrees with published axon size distributions, which give an average diameter of $\approx$ 1.18 μm in the posterior midbody, and $\approx$ 0.87 μm anterior midbody (23). In the human brain, Fig 4 shows that R_1s are lowest in the posterior midbody ($\approx$ 1.11 1/s) and greatest in the splenium ($\approx$ 1.14 1/s) and genu ($\approx$ 1.22 1/s). These observations are consistent with literature reports from histology (24,25), which showed average axon sizes of $\approx$ 5μm in the posterior midbody, $\approx$ 3.5 μm in the splenium, and $\approx$ 2.5 μm in the genu. The relationship between T_1 and axon size is also consistent with some previous quantitative measures of T_1 in human brain. Yarnykh et al. (26) showed relatively high T_1 in the corticospinal tract and medial lemniscus, both of which contain large myelinated axons (27,28), and relatively low T_1 values in the genu and splenium of the corpus callosum, known to be comprised largely of small diameter axons (24).

The physical explanation for the relationship between T_1 and axon diameter may be due to compositional variations of axoplasm related to axon size, but it is more likely still a myelin-

dependent phenomenon. If relaxation of intra- and extra-axonal water is dominated by water interaction with the inner and outer surfaces of the myelin, then larger diameter axons with a lower myelin surface-to-volume ratio (SVR) will result in lower rate of water-membrane interactions and a lower relaxation rate (or higher T_1) for a constant myelin volume fraction. A similar framework has been used to estimate compartment sizes in porous media (29,30); however, a complete model relating axon diameter to SVR (and, in-turn, the observed T_1) will be complicated by considering at least two distinct water compartments (intra- and extra-axonal) and the dependence of both axon density and g-ratio on axon diameter (31-33).

A second, similar explanation depends on the physical exchange of water between the myelin and non-myelin compartments. Given the aforementioned assumption that water in myelin relaxes with a relatively short T_1, the exchange of water between myelin and non-myelin compartments in white matter will serve to accelerate longitudinal relaxation of the longer-lived water signal, which may dominate most T_1 measurements. In this case, the ability for myelin water to reach intra- or extra-axonal space will affect T_1—larger axons and/or thicker myelin could result in a lower rate of water exchange between the myelin and non-myelin compartments, leading to a longer observed T_1 of the non-myelin water when compared to a tissue with the same amount of myelin but smaller axons or thinner myelin. This model is nuanced by the implicit assumption that the white matter water signal is bi-exponential as a result of water compartmentalization, but is typically measured as a mono-exponential, and despite some recent experimental studies supporting the effect of water exchange on T_2 (17,18,34), other work suggests that myelin water exchange in the brain is slow on a T_1 time scale (35).

Regardless of the details of the physical mechanisms causing the relationship between T_1 and axon size, the empirical relationship itself has important implications on MRI studies of white matter microstructure and composition. Some recent works (14,15) offer promise for using T_1 measurements to quantitatively map myelin content. This approach is attractive in its simplicity compared to more complex techniques such as qMT (19,36) or multi-exponential analysis (19,36), but the observations presented here indicate that interpreting T_1 differences between regions or subjects as necessarily reflective of differences in myelin content may not be correct in general. However, because T_1 is more sensitive to myelin content than axon size, T_1 mapping remains a fast and simple measure of myelin content for suitable many situations. Similarly, another approach to fast and simple myelin content mapping is through the use a calibrated ratio of gradient echo and turbo spin echo images (TSE) (37), which has recently been extended from cortical to whole brain myelin mapping (38). The idea behind this approach is that myelin increases signal in T_1-weighted gradient echo images while decreasing signal in TSE images, so the ratio should scale with myelin content while cancelling spatial variations in signal intensity. Again, the observations on T_1 presented here, coupled with previous observations of the relationship between T_2 and axon diameter (17,18), suggest that this ratio will also be influenced by axon diameter.

If the effect of axon size on T_1 is substantial enough to significantly alter these T_1-based methods of myelin mapping, it may be that combining T_1 measurements with independent evaluations of axon diameter (23,39-41) may offer a novel and more robust approach to

quantitative myelin mapping, at least in the absence of inflammation or other pathology that independently alters T_1. Alternatively, combining T_1 measurements with an independent measure of myelin content, from, for example, qMT, may offer diffusion-free approach for estimating axon diameters in normal white matter. This idea is similar to the implications of previous studies showing a relationship between T_2 and axon diameter (17,18).

Acknowledgments

Grant sponsors: NIH R01 EB001744

REFERENCES

1. Bottomley PA, Foster TH, Argersinger RE, Pfeifer LM. A review of normal tissue hydrogen NMR relaxation times and relaxation mechanisms from 1-100 MHz: Dependence on tissue type, NMR frequency, temperature, species, excision and age. Med Phys. 1984; 11:425–448. [PubMed: 6482839]
2. Go K, Edzes H. Water in Brain Edema. Observations by the Pulsed Nuclear Magnetic Resonance Technique. Arch. Neurol. 1975; 32:462–465. [PubMed: 1137512]
3. Koenig SH, Brown RD, Spiller M, Lundbom N. Relaxometry of brain: why white matter appears bright in MRI. Magn. Reson. Med. 1990; 14:482–95. [PubMed: 2355830]
4. Does MD, Gore JC. Compartmental Study of T_1 and T_2 in Rat Brain and Trigeminal Nerve In Vivo. Magn. Reson. Med. 2002; 47:274–283. [PubMed: 11810670]
5. Lancaster JL, Andrews T, Hardies LJ, Dodd S, Fox PT. Three-pool model of white matter. J. Magn. Reson. Imaging. 2003; 17:1–10. [PubMed: 12500269]
6. Stanisz G, Kecojevic A, Bronskill M, Henkelman R. Characterizing White Matter with Magnetization Transfer and T_2. Magn. Reson. Med. 1999; 42:1128–1136. [PubMed: 10571935]
7. Travis AR, Does MD. Selective excitation of myelin water using inversion-recovery-based preparations. Magn. Reson. Med. 2005; 54:743–7. [PubMed: 16088884]
8. Levene M, Whitelaw A, Dubowitz V, Bydder G, Steiner R, Randell C, Young I. Nuclear magnetic resonance imaging of the brain in children. Br. Med. J. 1982; 285:774–776. [PubMed: 6810994]
9. Holland B, Haas D, Norman D, Brant-Zawadzki M, Newton T. MRI of normal brain maturation. Am. J. Neuroradiol. 1986; 7:201–208. [PubMed: 3082150]
10. Lacomis D, Osbakken M, Gross G. Spin-Lattice Relaxation (T_1) Times of Cerebral White Matter in Multiple Sclerosis. Magn. Reson. Med. 1986; 3:194–202. [PubMed: 3713485]
11. Bot J, Blezer E. The Spinal Cord in Multiple Sclerosis : Relationship of Quantitative MR Imaging Findings to Histopathologic Results. Radiology. 2004; 233:531–540. [PubMed: 15385682]
12. Mottershead JP, Schmierer K, Clemence M, et al. High field MRI correlates of myelin content and axonal density in multiple sclerosis--a post-mortem study of the spinal cord. J. Neurol. 2003; 250:1293–301. [PubMed: 14648144]
13. Schmierer K, Scaravilli F, Altmann DR, Barker GJ, Miller DH. Magnetization transfer ratio and myelin in postmortem multiple sclerosis brain. Ann. Neurol. 2004; 56:407–15. [PubMed: 15349868]
14. Stüber C, Morawski M, Schäfer A, et al. Myelin and iron concentration in the human brain: A quantitative study of MRI contrast. Neuroimage. 2014; 93:95–106. [PubMed: 24607447]
15. Callaghan MF, Helms G, Lutti A, Mohammadi S, Weiskopf N. A general linear relaxometry model of R_1 using imaging data. Magn. Reson. Med. 2014:00.
16. Brownstein K, Tarr C. Spin-lattice relaxation in a system governed by diffusion. J. Magn. Reson. 1977; 26:17–24.
17. Dula AN, Gochberg DF, Valentine HL, Valentine WM, Does MD. Multiexponential T_2, magnetization transfer, and quantitative histology in white matter tracts of rat spinal cord. Magn. Reson. Med. 2010; 63:902–9. [PubMed: 20373391]

18. Harkins KD, Dula AN, Does MD. Effect of intercompartmental water exchange on the apparent myelin water fraction in multiexponential T_2 measurements of rat spinal cord. Magn. Reson. Med. 2012; 67:793–800. [PubMed: 21713984]
19. Gochberg DF, Gore JC. Quantitative magnetization transfer imaging via selective inversion recovery with short repetition times. Magn. Reson. Med. 2007; 57:437–41. [PubMed: 17260381]
20. Viola P, Wells W. Alignment by Maximization of Mutual Information. Int. J. Comput. Vis. 1997; 24:1–29.
21. Li K, Zu Z, Xu J, Janve V a, Gore JC, Does MD, Gochberg DF. Optimized inversion recovery sequences for quantitative T_1 and magnetization transfer imaging. Magn. Reson. Med. 2010; 64:491–500. [PubMed: 20665793]
22. Thiessen JD, Zhang Y, Zhang H, Wang L, Buist R, Del Bigio MR, Kong J, Li X-M, Martin M. Quantitative MRI and ultrastructural examination of the cuprizone mouse model of demyelination. NMR Biomed. 2013; 26:1562–81. [PubMed: 23943390]
23. Barazany D, Basser PJ, Assaf Y. In vivo measurement of axon diameter distribution in the corpus callosum of rat brain. Brain. 2009; 132:1210–20. [PubMed: 19403788]
24. Aboitiz F, Scheibel AB, Fisher RS, Zaidel E. Fiber composition of the human corpus callosum. Brain Res. 1992; 598:143–153. [PubMed: 1486477]
25. Alexander DC, Hubbard PL, Hall MG, Moore E a, Ptito M, Parker GJM, Dyrby TB. Orientationally invariant indices of axon diameter and density from diffusion MRI. Neuroimage. 2010; 52:1374–89. [PubMed: 20580932]
26. Yarnykh VL, Yuan C. Cross-relaxation imaging reveals detailed anatomy of white matter fiber tracts in the human brain. Neuroimage. 2004; 23:409–24. [PubMed: 15325389]
27. Guyton, A.; Hall, J. Textbook of medical physiology. 10 ed.. W.B. Saunders; Philedelphia: 2000. p. 637
28. Swenson, R. Review of Clinical and Functional Neuroscience. 2006. Chapter 7
29. Brownstein KR, Tarr C. Importance of classical diffusion in NMR studies of water in biological cells. Phys. Rev. A. 1979; 19:2446–2453.
30. Kleinberg R, Kenyon W, Mitra P. Mechanism of NMR Relaxation of Fluids in Rock. J. Magn. Reson. 1994:206–14.
31. Berthold C, Nilsson I, Rydmark M. Axon diameter and myelin sheath thickness in nerve fibres of the ventral spinal root of the seventh lumbar nerve of the adult and developing cat. J. Anat. 1983; 136:483–508. [PubMed: 6885614]
32. Chatzopoulou E, Miguez A, Savvaki M, et al. Structural requirement of TAG-1 for retinal ganglion cell axons and myelin in the mouse optic nerve. J. Neurosci. 2008; 28:7624–36. [PubMed: 18650339]
33. Crawford DK, Mangiardi M, Song B, Patel R, Du S, Sofroniew MV, Voskuhl RR, Tiwari-Woodruff SK. Oestrogen receptor beta ligand: a novel treatment to enhance endogenous functional remyelination. Brain. 2010; 133:2999–3016. [PubMed: 20858739]
34. Dortch RD, Harkins KD, Juttukonda MR, Gore JC, Does MD. Characterizing intercompartmental water exchange in myelinated tissue using relaxation exchange spectroscopy. Magn. Reson. Med. 2013:1450–9. [PubMed: 23233414]
35. Labadie C, Lee J-H, Rooney WD, Jarchow S, Aubert-Frécon M, Springer CS, Möller HE. Myelin water mapping by spatially regularized longitudinal relaxographic imaging at high magnetic fields. Magn. Reson. Med. 2014; 71:375–87. [PubMed: 23468414]
36. Sled JG, Pike GB. Quantitative interpretation of magnetization transfer in spoiled gradient echo MRI sequences. J. Magn. Reson. 2000; 145:24–36. [PubMed: 10873494]
37. Glasser MF, Van Essen DC. Mapping human cortical areas in vivo based on myelin content as revealed by T_1- and T_2-weighted MRI. J. Neurosci. 2011; 31:11597–616. [PubMed: 21832190]
38. Ganzetti M, Wenderoth N, Mantini D. Whole brain myelin mapping using T_1- and T_2-weighted MR imaging data. Front. Hum. Neurosci. 2014; 8:671. [PubMed: 25228871]
39. Assaf Y, Blumenfeld-Katzir T, Yovel Y, Basser PJ. AxCaliber: a method for measuring axon diameter distribution from diffusion MRI. Magn. Reson. Med. 2008; 59:1347–54. [PubMed: 18506799]

40. Alexander DC. A general framework for experiment design in diffusion MRI and its application in measuring direct tissue-microstructure features. Magn. Reson. Med. 2008; 60:439–48. [PubMed: 18666109]

41. Xu J, Li H, Harkins KD, Jiang X, Xie J, Kang H, Does MD, Gore JC. Mapping mean axon diameter and axonal volume fraction by MRI using temporal diffusion spectroscopy. Neuroimage. 2014; 103C:10–19. [PubMed: 25225002]

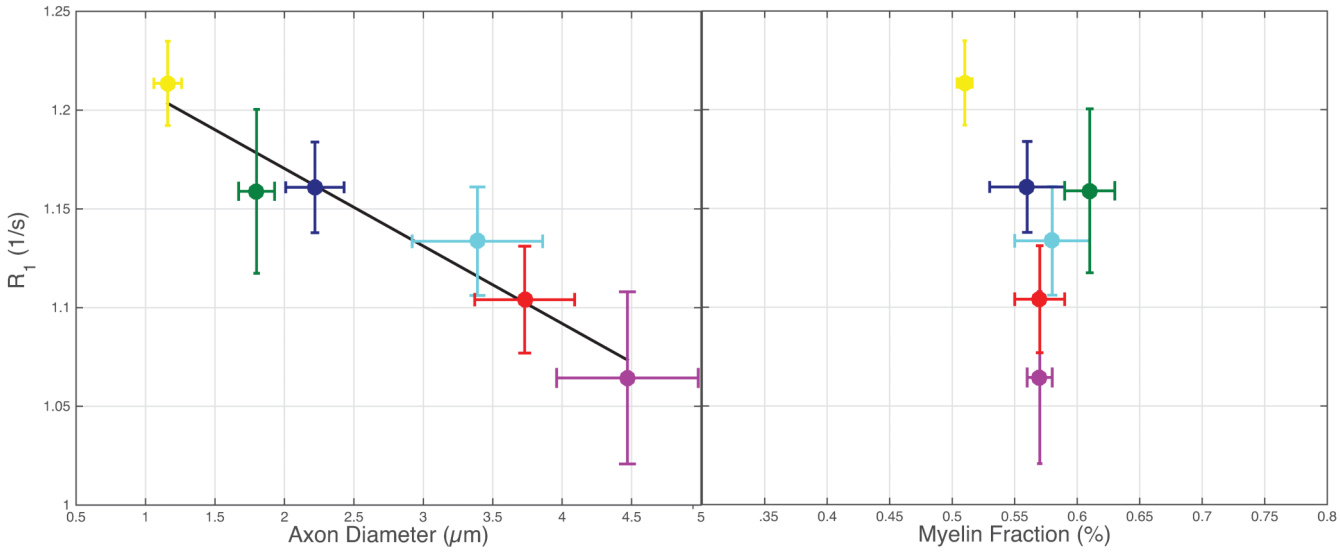

Figure 1.

A significant linear correlation is present between MR measured R_1 and histology derived mean axon diameter (R^2=0.93, P=0.002), while no such relationship is apparent between R_1 and myelin fraction (R^2=0.20, P=0.380). Yellow = dCST, green = FG, blue = ReST, teal = RST, red = FC, and purple = VST.

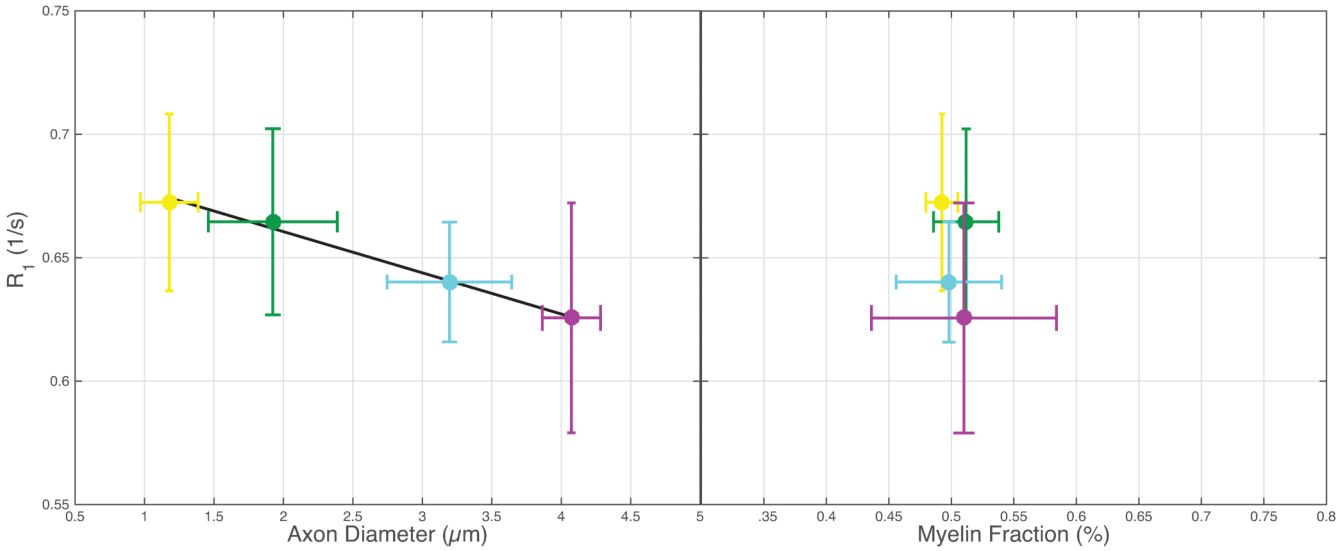

Figure 2.

Similar to the ex vivo data shown in Fig 1, there is a significant linear correlation between R_1 and mean axon diameter ($R^2 = 0.98$, P=0.006), while no trend is evident with myelin fraction ($R^2 = 0.16$, P=0.600). Colors in all sub-figures are matched to the colors given in Fig 1.

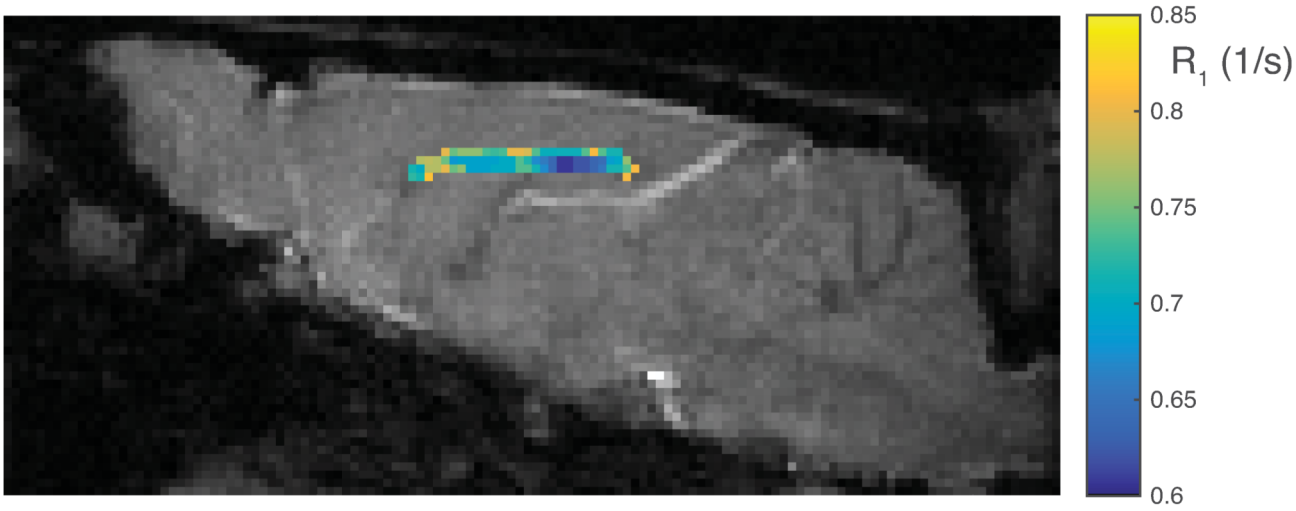

Figure 3.

A gradient echo image of a sagittal slice through the center of the rat brain, with a color overlay of R_1 through the corpus callosum.

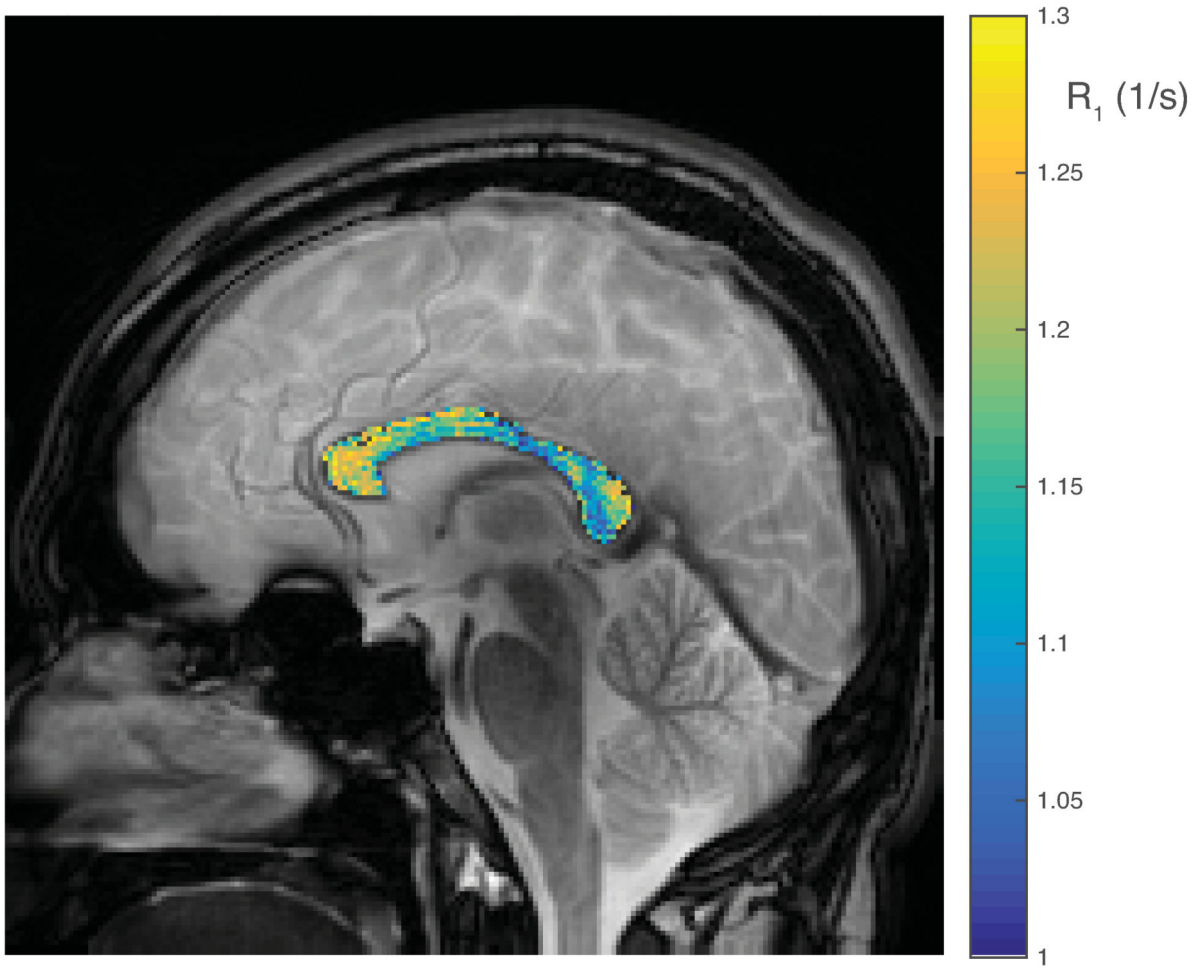

Figure 4.

A gradient echo image of a sagittal slice through the center of the human brain, with a color overlay of R_1 through the corpus callosum.

Table 1

Histologically derived axon diameter (AxD) and myelin fraction (MF) as well as qMT measured T_1, and pool size ratio (PSR) within several spinal cord tracts in ex vivo and in vivo rat studies.

	Ex vivo			
	AxD (μm)	**MF**	**T_1 (s)**	**PSR**
dCST	1.160 (0.100)	0.510 (0.006)	0.824 (0.015)	0.237 (0.013)
FG	1.800 (0.130)	0.610 (0.020)	0.864 (0.032)	0.244 (0.013)
ReST	2.220 (0.210)	0.560 (0.030)	0.862 (0.017)	0.245 (0.011)
RST	3.390 (0.470)	0.580 (0.030)	0.883 (0.022)	0.234 (0.012)
FC	3.730 (0.360)	0.570 (0.020)	0.906 (0.022)	0.227 (0.019)
VST	4.470 (0.510)	0.570 (0.010)	0.941 (0.038)	0.234 (0.009)

	In vivo			
dCST	1.178 (0.208)	0.492 (0.013)	1.491 (0.085)	0.157 (0.020)
FG	1.924 (0.465)	0.512 (0.026)	1.509 (0.089)	0.176 (0.035)
RST	3.196 (0.449)	0.498 (0.042)	1.564 (0.059)	0.142 (0.016)
VST	4.074 (0.209)	0.510 (0.074)	1.607 (0.128)	0.163 (0.023)